

# Experimental investigation of 3-D surface microtexture of nickel-carbon nanocomposite thin films

Ștefan Țălu, Alicja Rąplewicz, Sebastian Stach

**Abstract.** The study's aim was to identify the 3-D surface spatial parameters that describe the 3-D surface microtexture of the nickel-carbon (Ni-C) nanocomposite thin films composed of Ni nanoparticles with different average sizes embedded in amorphous hydrogenated carbon, prepared by the combining radio frequency magnetron sputtering technique and plasma-enhanced chemical vapor deposition (RF-PECVD). The deposition time was varied at 7, 10 and 13 min, respectively. The sample investigation was performed using an atomic force microscope, and the obtained data were analyzed and visualized using MountainsMap® Premium software to determine their stereometric surface engineering characteristics. The results from this study provide not only fundamental insights into the texture characteristics, but also directions toward their implementation in nano-tribological models

## I. INTRODUCTION

In the field of nanotechnology, the investigative tools and level of understanding of basic nanoscale phenomena has led to the optimization of nanostructure properties, the correct understanding of the thin film growth mechanism, as well as finding of new applications with high impact in the areas of energy, environment, communications, computing, medicine, space exploration, and security [1]-[7].

A key element in the manufacturing process is the application of a method to obtain the optimal nanostructure through a no-bake step [8]-[11].

The thin films can be rationally designed to exhibit novel and significantly improved physical, chemical, mechanical and magnetic properties [12]-[22].

Ștefan Țălu is with the Technical University of Cluj-Napoca, The Directorate of Research, Development and Innovation Management (DMCDI), Constantin Daicoviciu Street, no. 15, Cluj-Napoca, 400020, Cluj county, Romania, [stefan\\_ta@yahoo.com](mailto:stefan_ta@yahoo.com)

Alicja Rąplewicz and Sebastian Stach are with the University of Silesia, Faculty of Computer Science and Materials Science, Institute of Informatics, Department of Biomedical Computer Systems, Będzińska 39, 41-205 Sosnowiec, Poland

Diamond-like carbon (DLC) is metastable, amorphous carbon material, which may contain microcrystalline phase of diamond [23].

These films due to their attractive properties as coating materials have many fields of application in engineering, and medical technology [24]-[33].

Nickel as carbon composite has found many applications in many fields such as the optical coatings, catalyst, and water splitting electrode [34]-[38] and also along with carbon can have interesting physical properties [39]-[40].

The objective of this work was to characterize the 3-D surface microtexture of the Ni-C nanocomposite thin films with different mean grain sizes prepared by RF-PECVD using atomic force microscopy (AFM).

## II MATERIALS AND METHODS

### Ii.a.SAMPLES PREPARATION

Ni-C composite thin films were prepared by the methodology described in Ref. [2] with the synthetic conditions for preparing the samples according to Table I.

**Table 1.** Synthetic conditions used for preparing the samples.

ID	Tar-get	Sputtering parameters			Deposi-tion time [min]
		Basic preassure [mbar]	Working preassure [mbar]	Power [W]	
#1	Ni	10 <sup>-5</sup>	0.025	250	7
#2	Ni	10 <sup>-5</sup>	0.025	250	10
#3	Ni	10 <sup>-5</sup>	0.025	250	13

### Ii.b. MEASURING DATA ACQUISITION

The samples 1, 2 and 3 were analyzed by MountainsMap® Premium program version 6.2.7200 developed by Digital Surf [41]. All images were obtained over square areas of 1 μm x 1 μm.

The experimental data obtained using the atomic force microscopy was loaded into the MountainsMap®

Premium program and then leveled to remove the tilt of the image.

As the leveling method, the LS plane was selected, the leveling was done by the subtraction, which is a method suitable for small tilt angles.

This operation was performed for three samples labeled 1A (Fig. 1), 2A (Fig. 2), and 3A (Fig. 3).

The images of the samples 1, 2 and 3, before (top) and after the leveling operation (bottom) are shown in Figs. 1 to Fig. 3.

a) Sample 1

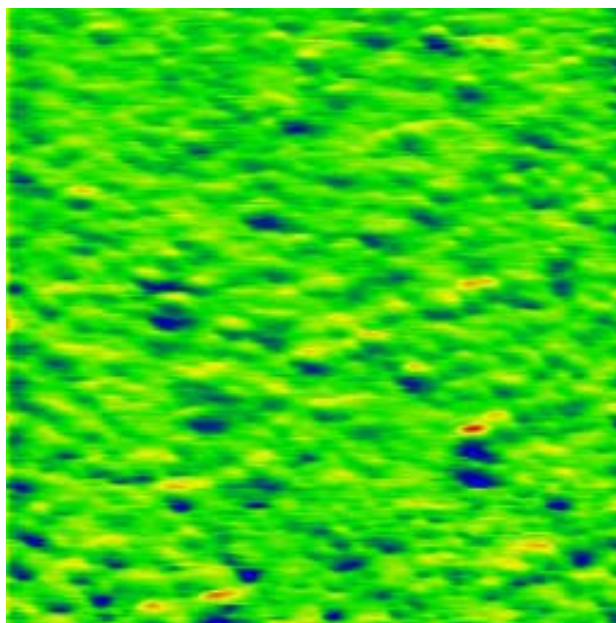


**Fig. 1, a.** The image of the sample 1 before the leveling operation.

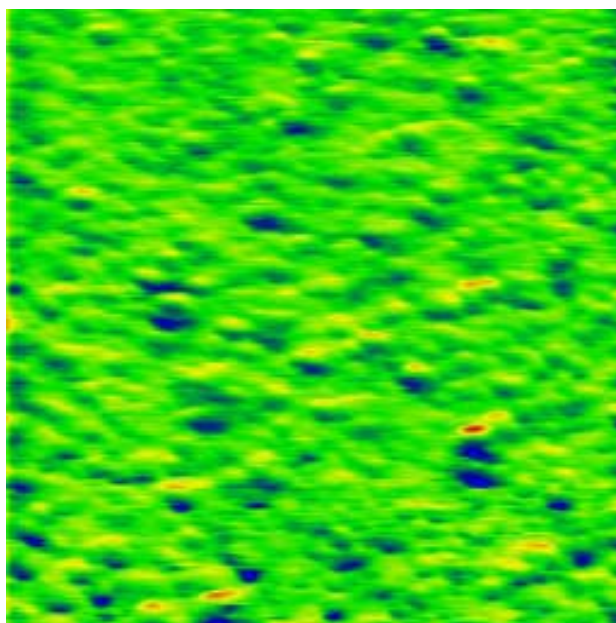


**Fig. 1, b.** The image of the sample 1 after the levelling operation.

b) Sample 2

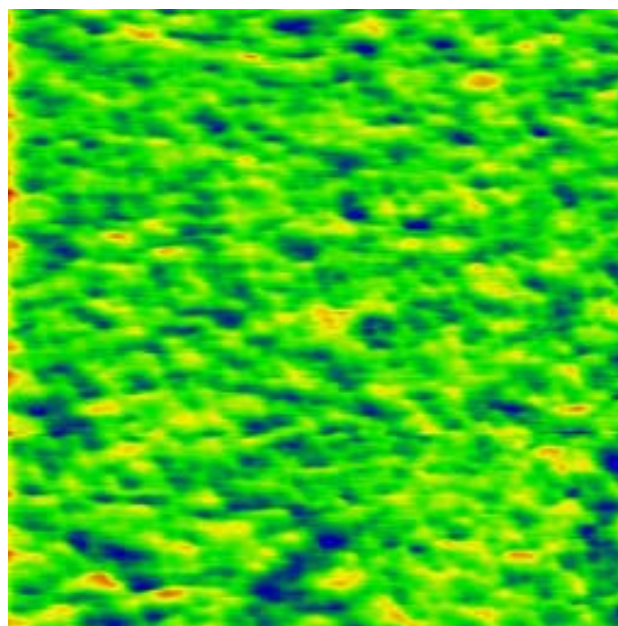


**Fig. 2, a.** The image of the sample 2 before the leveling operation.

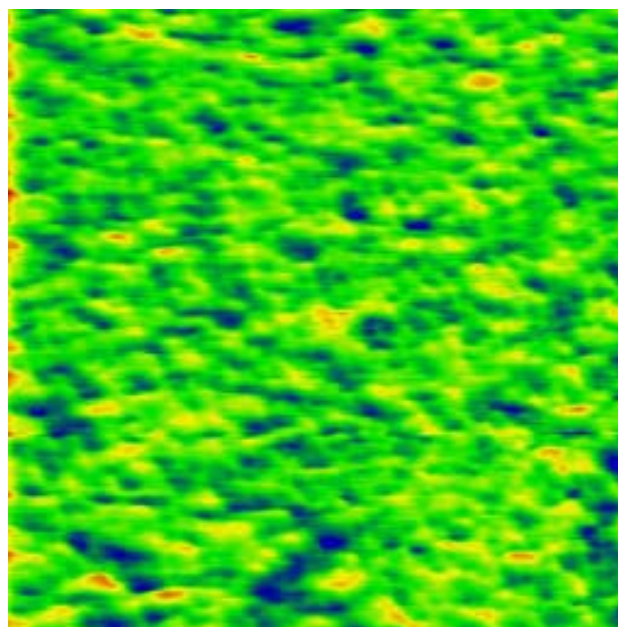


**Fig. 2, b.** The image of the sample 2 after the leveling operation.

c) Sample 3

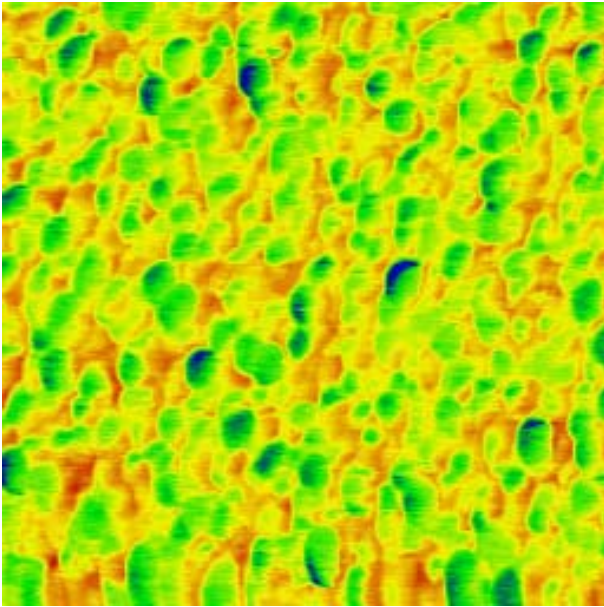


**Fig. 3, a.** The image of the sample 3 before the leveling operation.

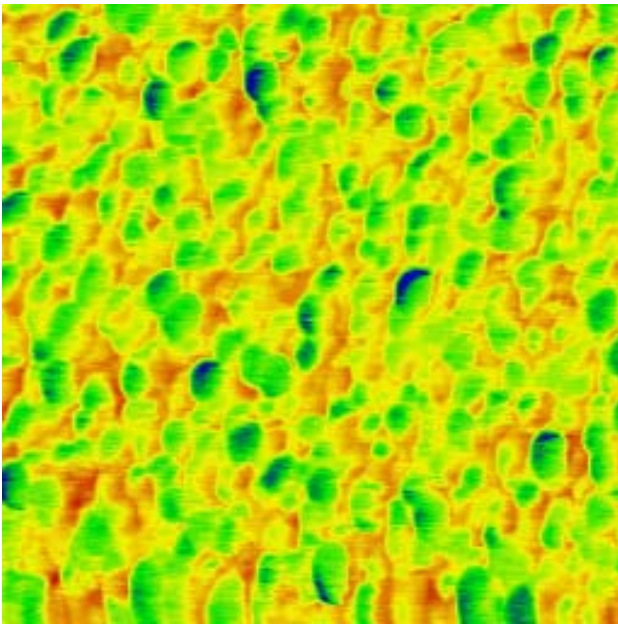


**Fig. 3, b.** The image of the sample 3 after the leveling operation.

Once a leveled image of each sample was obtained, another shape removal operation was performed. As with leveling, this operation was repeated for all three samples: 1 (Fig. 4, a), 2 (Fig. 4, b), and 3 (Fig. 4, c).

a) Sample 1

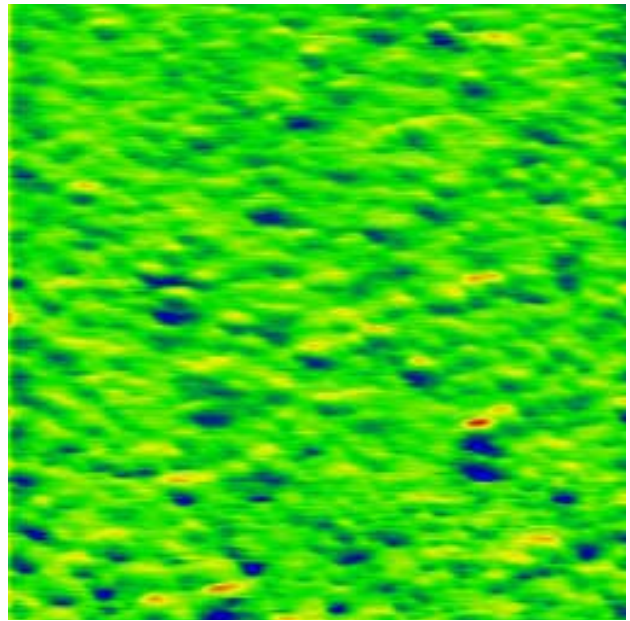


**Fig. 4, a.** The image of the sample 1 after shape removal operation.

b) Sample 2

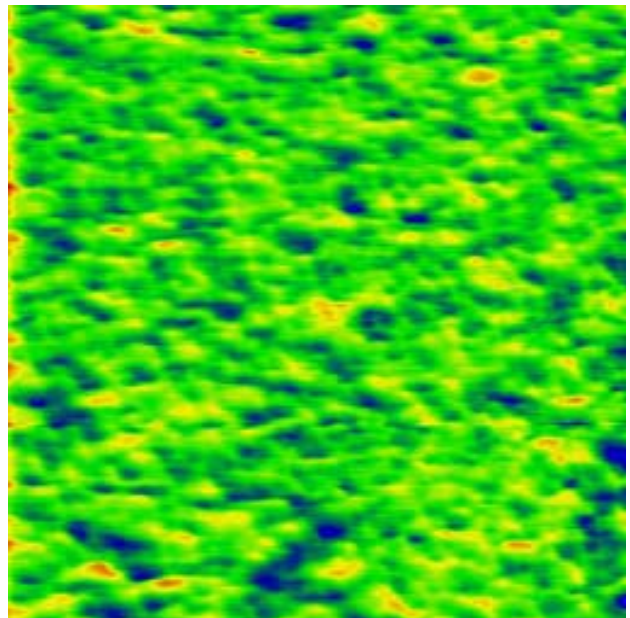


**Fig. 4, b.** The image of the sample 2 after shape removal operation.

c) Sample 3

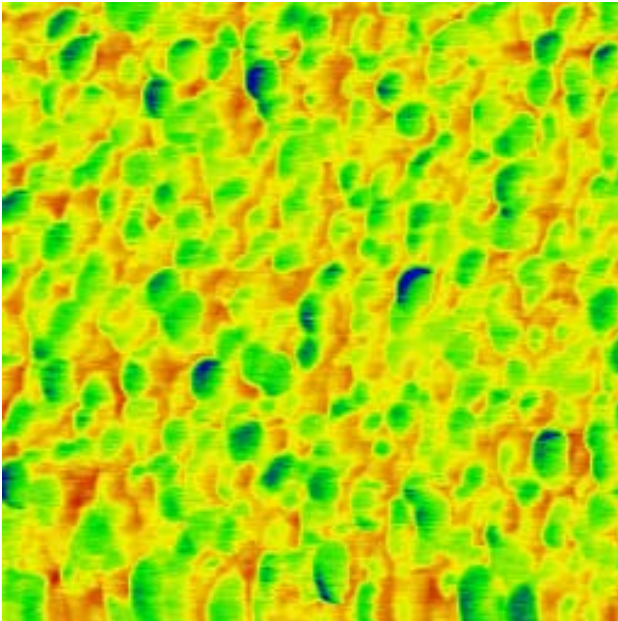


**Fig. 4, c.** The image of the sample 3 after shape removal operation.

The 3-D view of the investigated surface was generated for each sample, with the additional elements such as pitch, axis arrangement, and the dimensions (Fig. 5).

a) Sample 1

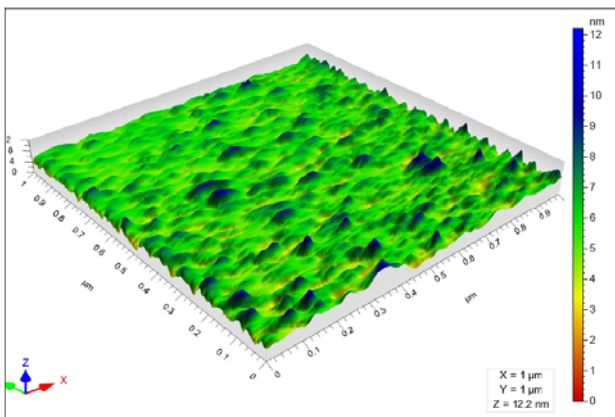


**Fig. 5, a.** The 3-D surface microtexture of the sample 1.

b) Sample 2

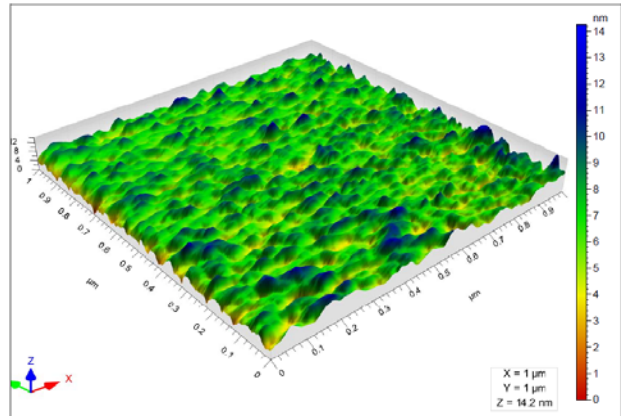


**Fig. 5, b.** The 3-D surface microtexture of the sample 2.

c) Sample 3

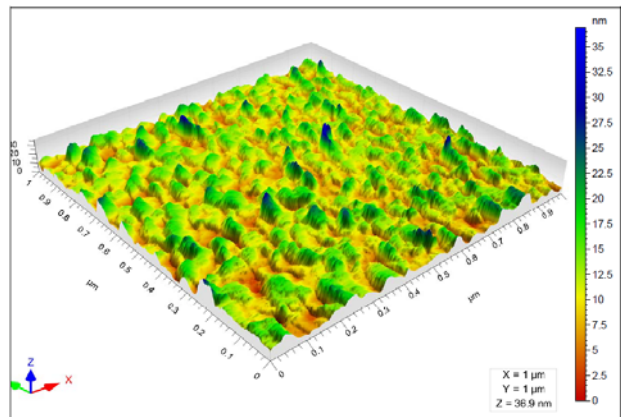


**Fig. 5, c.** The 3-D surface microtexture of the sample 3.

The ID cards were generated for each sample. These cards contain the most important information such as length, size, spacing, etc. The obtained data are summarized in the Table 2.

**Table 2.** Data from sample ID cards.

		Sample 1	Sample 2	Sample 3
Axis X	Length [μm]	1.00	1.00	1.00
	Size [points]	256	256	256
	Spacing [nm]	3.92	3.92	3.92
	Offset [μm]	0.00	0.00	0.024
Axis Y	Length [μm]	1.00	1.00	1.00
	Size [lines]	256	256	256
	Spacing [nm]	3.92	3.92	3.92
	Offset [μm]	-1.10	-1.00	-1.02
Axis Z	Length [nm]	12.2	14.2	36.9
	Z min [nm]	-5.71	-6.8	-11.6
	Z max [nm]	6.48	7.44	25.3
	Size [decimal place values]	159160	905994	134987
	Spacing [pm]	0.0766	0.0157	0.273

**Table 3.** Surface spatial parameters of the analyzed samples.

Parameters ID	Sample 1	Sample 2	Sample 3
Auto-correlation length Sal [ $\mu\text{m}$ ]	0.0139	0.0164	0.0202
Texture aspect ratio Str	0.362	0.429	0.510
Texture direction Std [ $^\circ$ ]	170	177	78.5

### III. ANALYSIS AND RESULTS

The sample investigations using AFM combined with the data processing with the MountainsMap<sup>®</sup> Premium program, enable the detailed and accurate analysis of the material surface.

On the basis of the performed measurements, it can be seen that parameters such as length, size or spacing for the X and Y axes are identical for each sample.

However, the offset is different: for the X axis is (0.00  $\mu\text{m}$ ) for samples 1 and 2, but it is 0.024  $\mu\text{m}$  for sample 3.

In the case of the Y axis, the value of the offset is negative in all cases, but this value varies slightly from sample to sample, for the sample 1 it becomes value (-1.1  $\mu\text{m}$ ), for the sample 2 (-1.00  $\mu\text{m}$ ), and for sample 3 (-1.02  $\mu\text{m}$ ).

The greatest differences can be observed in the case of Z axis. The largest axis length (36.9 nm) is observed for the sample 3, while the shortest length of Y axis is (12.2 nm) for the sample 1. The middle value (14.2 nm) is measured for the sample 2. It can be deduced that the shorter the deposition time of a particular sample, the smaller the thickness of the resulting material.

Therefore, there are also differences in the minimum and maximum values measured for the Z axis. All the minimum values assume negative values. The difference between the smallest and the highest minimum value on the Z axis accepted for the individual samples is (5.89 nm). The smallest value was observed for sample 1 (-5.71 nm), while the largest for sample 3 (-11.6 nm).

The midpoint (-6.8 nm) was observed for sample 2. The maximum values, measured for the individual samples on the Z axis, all are positive, where the difference between the smallest and the highest values is observed (18.32 nm). The smallest value (6.48 nm) is measured for sample 1, while the largest (25.3 nm) for sample 3. The middle value is observed for the sample 2, for which Z is the maximum (7.44 nm).

Other differences to observe based on the performed research and analysis are the variations in the size of each sample on the Z axis. The difference between the largest and the smallest sample size is 746834 decimal places. The smallest value is observed for sample 3, the size of which is (134987 decimal places), while the highest value (905994 decimal places) is measured for sample 2. The middle value (159160 decimal places) is measured for sample 1.

Therefore it can be assumed that there is some dependence between the deposition time and the sample size on the Z axis. However, this is not proportional in any way, because the shortest deposition time is observed for the investigated sample with the mean size, and the longest deposition time for the sample with the smallest size of the Z axis. On the other hand, the largest sample size was measured for a sample with an average deposition time. Similar dependencies observed in case of the spacing. The difference between the smallest and the largest spacing is (0.2573 pm). The largest spacing (0.273 pm) is observed for sample 3, while the smallest Z axis spacing (0.01575 pm) is measured for 2. The center value of the spacing (0.0766 pm) was measured for sample 1.

During the study, spatial parameters were also analyzed in accordance with ISO 25178. Through this analysis, the effect of the deposition time and the surface parameters such as the autocorrelation length, the texture aspect ratio and the texture direction can be observed. Depending on the time of the thin film deposition, an increase in the autocorrelation length can be observed. The difference between two extremes is (0.0063  $\mu\text{m}$ ). The smallest value of the Sal (0.0139  $\mu\text{m}$ ), is measured for sample 1 and the highest value (0.0202  $\mu\text{m}$ ) is taken for sample 3. The average value (0.0164  $\mu\text{m}$ ) is observed for sample 2. It can be observed that the longer the deposition time of a sample, the higher the Sal factor, i.e. the deposition time of the sample significantly affects the longevity of the surface of the material - the longer the deposition time, the longer the surface of the sample.

Another parameter, which significantly influences the time of film deposition, is the texture aspect ratio Str. The difference between the highest and lowest value of this parameter is (0.148). Similar to the case of the autocorrelation length, the smallest value (0.362) is obtained for the sample 1, while for sample 3 is measured the highest value of this parameter (0.510). The average value of (0.429) is observed for the sample 2.

It can be noted that the deposition time affects the isotropy of the material surface. The shorter the deposition time, the surface of the obtained material shows less anisotropy. Due to the lack of the anisotropy in the tested samples, it was possible to determine the texture direction. The difference between extreme values is (98.5 $^\circ$ ). The smallest value (78.5 $^\circ$ ) is measured for the sample 3, while the largest (177 $^\circ$ ) is observed for the sample 2. The sample 1 assumes a center value of the texture direction (170 $^\circ$ ).

### VI. CONCLUSION

The objective of this study was to characterize the surface micromorphology of the nickel-carbon nanocomposite thin films composed of Ni nanoparticles with different average sizes embedded in amorphous hydrogenated carbon, prepared by RF-PECVD. The AFM sample images were processed using MountainsMap<sup>®</sup> Premium program.

Analysis of the results obtained using the MountainsMap<sup>®</sup> Premium program was based on the

leveling and shaping operations for each sample, as well as generating three-dimensional views of the surfaces of the analyzed materials, together with all necessary scales and legends.

In addition, were generated ID cards which contain all the basic data of the investigated samples. The spatial parameters values according to ISO 25178 were also evaluated.

Such detailed investigations of material parameters, not only spatial, have an extraordinary potential and a multitude of the applications. An accurate surface analysis can greatly facilitate the engineering design process, especially for the items such as implants and prostheses, which require the special attention and precision. In addition, the investigation of the materials in nanoscale may be very useful for the study of the friction wear or the effects of body fluids on the particular material properties.

Our analysis revealed there is an influence of the deposition time of the material on its three-dimensional geometry. The greatest influence can be observed in the case of the Z axis of the examined samples and in the case of spatial parameters used to describe the surface of the material. The deposition time significantly affects the thickness of the resulting material, as well as its isotropy and long-term surface area of the nickel-carbon composite. Such detailed investigations in nanoscale of material parameters, not only spatial, have an extraordinary potential and a multitude of the applications. An accurate surface analysis can greatly facilitate the engineering design process.

## Appendix

The spatial parameters of 3D surface roughness, according with ISO 25178-2: 2012 are defined as follows [42]:

Spatial parameters describe topographic characteristics based upon spectral analysis. They quantify the lateral information present on the X- and Y-axes of the surface.

(Sal) - Auto-correlation length is the horizontal distance of the autocorrelation function ( $t_x$ ,  $t_y$ ) which has the fastest decay to a specified value  $s$ , with  $0 < s < 1$ . The default value for  $s$  in the software is 0.2. This parameter expresses the content in wavelength of the surface. A high value indicates that the surface has mainly high wavelengths (low frequencies). In our study,  $s = 0.2$ .

(Str) - Texture-aspect ratio is the ratio of the shortest decrease length at 0.2 from the autocorrelation, on the greatest length. This parameter has a result between 0 and 1. If the value is near 1, we can say that the surface is isotropic, i.e. has the same characteristics in all directions. If the value is near 0, the surface is anisotropic, i.e. has an oriented and/or periodical structure. In our study,  $s = 0.2$ .

(Std) - Texture direction calculates the main angle for the texture of the surface, given by the maximum of the polar spectrum. This parameter has a meaning if Str is lower than 0.5. In our study, Reference Angle =  $0^\circ$ .

The authors would like to thank to PhD. Ali Arman, Young

Researchers and Elite Club, Arak Branch, Islamic Azad University, Arak, Iran, for his helpful advice and stimulating discussions during this study.

## References

1. Y. Lei, W.K. Chim, J. Am. Chem. Soc. **127**(5), 1487–1492 (2005). DOI: 10.1021/ja043969m
2. S. Stach, Ž. Garczyk, Ş. Țălu, S. Solaymani, A. Ghaderi, R. Moradian, N.B. Nezafat, S.M. Elahi, H. Gholamali, J. Phys. Chem. C, **119**(31), 17887–17898 (2015). DOI: 10.1021/acs.jpcc.5b04676
3. Ş. Țălu, C. Luna, A. Ahmadpourian, A. Achour, A. Arman, S. Naderi, N. Ghobadi, S. Stach, B. Safibonab, J. Mater. Sci. Mater. Electron, **27**(11), 11425–11431 (2016). DOI: 10.1007/s10854-016-5268-9
4. S. Stach, W. Sapota, Ş. Țălu, A. Ahmadpourian, C., Luna, N. Ghobadi, A. Arman, M. Ganji, J. Mater. Sci. Mater. Electron, **28**(2), 2113–2122 (2016)
5. Ş. Țălu, *Micro and nanoscale characterization of three dimensional surfaces. Basics and applications* (Cluj-Napoca, Romania: Napoca Star Publishing House, 2015)
6. M. Molamohammadi, C. Luna, A. Arman, S. Solaymani, A. Boochani, A. Ahmadpourian, A. Shafiekhani, J. Mater. Sci. Mater. Electron, **26**(9), 6814–6818 (2015). DOI: 10.1007/s10854-015-3294-7
7. Ş. Țălu, S. Stach, A. Méndez, G. Trejo, M. Țălu, J Electrochem Soc., **161**, D44–D47 (2014).
8. A. Arman, Ş. Țălu, C. Luna, A. Ahmadpourian, M. Naseri, M. Molamohammadi, J. Mater. Sci. - Mater. Electron., **26**(12), 9630–9639 (2015)
9. S. Ramazanov, Ş. Țălu, D. Sobola, S. Stach, G. Ramazanov, Superlattices Microstruct., **86**, 395–402 (2015). DOI: 10.1016/j.spmi.2015.08.007
10. Ş. Țălu, S. Stach, D. Raoufi, F. Hosseinpanahi, Electron. Mater. Lett, **11**(5), 749–757 (2015). DOI: 10.1007/s13391-015-4280-1
11. S. Stach, D. Dallaeva, Ş. Țălu, P. Kaspar, P. Tománek, S. Giovanzana, L. Grmela, Mater. Sci. Poland, **33**(1), 175–184 (2015)
12. Ş. Țălu, A.J. Ghazai, S. Stach, A. Hassan, Z. Hassan, M. Țălu, J. Mater. Sci. Mater. El., **25**(1), 466–477 (2014). DOI: 10.1007/s10854-013-1611-6
13. Ş. Țălu, S. Stach, S. Valedbagi, S.M. Elahi, R. Bavadi, Mater. Sci. Poland, **33**(1), 137–143 (2015). DOI: 10.1515/msp-2015-0010
14. D. Dallaeva, Ş. Țălu, S. Stach, P. Škarvada, P. Tománek, L. Grmela, Appl. Surf. Sci., **312**, 81–86 (2014). DOI: 10.1016/j.apsusc.2014.05.086
15. N. Ghobadi, M. Ganji, C. Luna, A. Arman, A. Ahmadpourian, J. Mater. Sci. Mater. Electron, **27**(3), 2800–2808 (2016). DOI: 10.1007/s10854-015-4093-x
16. Ş. Țălu, S. Stach, S. Solaymani, R. Moradian, A. Ghaderi, M.R. Hantehzadeh, S.M. Elahi, Ž. Garczyk, S. Izadyar, J Electroanal. Chem., **749**, 31–41 (2015). DOI: 10.1016/j.jelechem.2015.04.009

17. T. Ghodselahi, A. Arman, *J. Mater. Sci. Mater. Electron*, **26**(6), 4193–4197 (2015). DOI: 10.1007/s10854-015-2965-8
18. A. Ahmadpourian, C. Luna, A. Boochani, A. Arman, A. Achour, S. Rezaee, S. Naderi, *EPJ Plus*, **131**(10), 381 (2016). DOI: 10.1140/epjp/i2016-16381-2
19. N. Ghobadi, M. Ganji, C. Luna, A. Ahmadpourian, A. Arman, *Opt Quant Electron*, **48**(10), 467 (2016). DOI: 10.1007/s11082-016-0742-4
20. A. Arman, C. Luna, M. Mardani, F. Hafezi, A. Achour, A. Ahmadpourian, *J. Mater. Sci. Mater. Electron*, **28**(6), 4713–4718 (2017)
21. S. Naderi, A. Ghaderi, S. Solaymani, M.M. Golzan, *EPJ AP*, **58**(2), 20401 (2012). DOI: 10.1051/epjap/2012110310
22. V. Dalouji, S.M. Elahi, S. Naderi, *Rare Metals*, **35**(11), 863-869 (2016). DOI: 10.1007/s12598-015-0581-7
23. P. Gupta, *Synthesis, Structure and Properties of Nanolayered DLC/DLC films* (MSc Thesis, Louisiana State University, May 2003)
24. R. Hauert, *Tribology International*, **37**(11), 991-1003 (2004). DOI: 10.1016/j.triboint.2004.07.017
25. R. Hauert, *Diam Relat Mater*, **12**(3), 583-589 (2003). DOI: 10.1016/S0925-9635(03)00081-5
26. A. Matthews, S.S. Eskildsen, *Diam Relat Mater*, **3**(4-6), 902-911 (1994). DOI: 10.1016/0925-9635(94)90297-6
27. F.Z. Cui, D.J. Li, *Surf. Coat. Technol.*, **131**, 481-487 (2000). DOI: 10.1016/S0257-8972(00)00809-4
28. S. V. Hainsworth, V. Sarah, N. J. Uhure, *Int. Mater. Rev.*, **52**(3), 153-174 (2007). DOI: 10.1179/174328007X160272
29. J.K. Luo, Y.Q. Fu, H.R. Le, J.A. Williams, S.M. Spearing, W.I. Milne, *J Micromech Microeng.*, **17**(7), S147 (2007). DOI: 10.1088/0960-1317/17/7/S12
30. A. Erdemir, C Donnet, *J Phys D Appl Phys*, **39**(18), R311 (2006). DOI: 10.1088/0022-3727/39/18/R01
31. S. Abdolghaderi, B. Astinchap, A. Shafiekhani, *J. Mater. Sci. Mater. Electron*, **27**(7), 6713–6720 (2016). DOI: 10.1007/s10854-016-4620-4
32. F. Mashayekhi, A. Shafiekhani, S.A. Sebt, *Eur. Phys. J. Appl. Phys.*, **74**, 30402 (2016). DOI: 10.1051/epjap/2016150508
33. M.A. Vesaghi, A. Shafiekhani, *J. Phys. D: Appl. Phys.*, **32**, L101 (1999). DOI: 10.1088/0022-3727/31/12/00
34. S.H. Jeong, B.S. Kim, B.T. Lee, J.K. Kim, H.R. Park, *J. Korean Phys. Soc.*, **41**(1), 67-72 (2002). Reference Number 35028993
35. B. Bayatsarmadi, Y. Zheng, V. Russo, L. Ge, C. S. S. Casari, S. Qiao, *Nanoscale*, **8**(43), 18507-18515 (2016). DOI: 10.1039/C6NR06961D
36. N. Bouts, M. Gaillard, L. Donero, A.A. El Mel, E. Gautron, B. Angleraud, C. Boulmer-Leborgne, P.Y. Tessier, *Thin Solid Films*, **630**, 38–47 (2017). DOI: 10.1016/j.tsf.2016.10.025
37. A. Arman, T. Ghodselahi, M. Molamohammadi, S. Solaymani, H. Zahrabi, A. Ahmadpourian, *Prot. Met. Phy. Chem*, **51**(4), 575–578 (2015)
38. M. Molamohammadi, A. Arman, A. Achour, B. Astinchap, A. Ahmadpourian, A. Boochani, S. Naderi, A. Ahmadpourian, *J. Mater. Sci. Mater. Electron*, **26**(8), 5964-5969, 2015
39. Harish C. Barshilia, K.S. Rajam, *Surf Coat Technol.*, **155**, 195-202 (2002). DOI: 10.1016/S0257-8972(02)00008-7
40. S.M. Cherif, A. Layadi, J. Ben Youssef, C. Nacereddine, Y. Roussigne, *Physica B*, **387**(1-2), 281-286 (2007). DOI: 10.1016/j.physb.2006.04.037
41. MountainsMap<sup>®</sup> 7 Software (Digital Surf, Besançon, France). Available from: <http://www.digitalsurf.fr> (last accessed April 25<sup>th</sup>, 2018)
42. ISO 25178-2: 2012 Geometrical product specifications (GPS) – Surface texture: Areal – Part 2: Terms, definitions and surface texture parameters. (2012) <http://www.iso.org>. (last accessed April 25<sup>th</sup>, 2018)